

UP- AND DOWNGOING GREEN'S FUNCTIONS RETRIEVED BY INVERSE WAVEFIELD EXTRAPOLATION

D. F. Barrera, J. Schleicher, and J. van der Neut

email: *df.barpa@gmail.com, js@ime.unicamp.br*

keywords: *Green's functions constituents, datum, one-way reciprocity theorems*

ABSTRACT

Inverse wavefield extrapolation methods are required in many imaging techniques. We propose a new methodology to recover the up- and downgoing wavefield components at a new datum in depth from surface seismic data after elimination of free-surface multiples. The procedure is based on the one-way reciprocity theorems of convolution and correlation type and makes use of two wavefield estimates that can be simulated with the knowledge of an overburden model only. The desired wavefield constituents at the datum are then obtained by solving the underlying equation system by means of stabilized least-squares inversion. Our numerical examples show that the procedure works as theoretically predicted and that it does not suffer from the kind of non-physical events that are common in correlation-based redatuming.

INTRODUCTION

Inverse wavefield extrapolation is a term used to describe the process of recovering the wavefield somewhere in depth from then recorded at the earth's surface, generally by retroproagation back into the earth (van der Neut et al., 2015b). This concept it is used in many imaging schemes, e.g., RTM (Kosloff and Baysal, 1983), interferometric redatuming (Schuster, 2009), Marchenko imaging (Wapenaar et al., 2014b) and others. Particularly, many works regarding the topic of Marchenko imaging, study and employ inverse wavefield extrapolation to recover so-called focusing functions, being considered the first iteration of this technique (van der Neut et al., 2015a). Conventional inverse wavefield extrapolation techniques have the drawback that the manipulated wavefields in the target area still carry information about the overburden. The very purpose of Marchenko imaging is to remove this influence, which generally leads to the presence of incorrectly treated multiples and other non-physical artefacts (van der Neut et al., 2014).

In this work, we propose a simpler alternative to the estimation of focusing functions in Marchenko imaging, which also allows to remove overburden multiples and spurious events from the Green's functions retrieved at a new datum in depth. The strength of the conventional procedure lies in the fact that it needs only an estimate of the transmitted wavefield from the earth's surface to the datum to recover the full wavefield there. However, this makes it a rather sophisticated method to retrieve the Green's functions at the datum. By using an additional wavefield estimate in the overburden, our procedure allows to determine the up- and downgoing constituents of the Green's functions at depth by means of a least-squares inversion. Note, however, that this will generally require a better model of the overburden inhomogeneities.

The underlying equations of our method are the one-way reciprocity theorems of convolution and correlation type. These two formulas can be reformulated in such a way that they allow to express the data at the surface as integrals over wavefields that propagate only in the overburden and the desired up- and downgoing wavefield constituents at the datum (van der Neut et al., 2015a). The two involved wavefields in the overburden are the transmitted wavefield from the surface to the datum, and the so-called truncated wavefield, i.e., the one reflected from the overburden scatterers only and recorded at the surface receivers. Both wavefields can be simulated in a reference model that is homogeneous below the datum. In this

work, we demonstrate the application of stabilized least-squares inversion to this equation system in order to retrieve these wavefield constituents. Our numerical examples show that the procedure works as theoretically predicted and that it does not suffer from the kind of non-physical events that are common in correlation-based redatuming (Barrera et al., 2016).

METHOD

In this section, we derive the reciprocity theorems using the Helmholtz equation with velocity and density variation. These derivations are fundamental to understand the wavefield expressions in different cases. The basic form, using a closed surface, is the ideal case for the reciprocity theorems, but special conditions make it possible to consider less ideal situations. Particularly, we focus on the one-way reciprocity theorems of correlation and convolution type. These theorems represent the platform upon which we derive the relationships allowing for up- and downward wavefield propagation with inversion.

In this work, the Fourier-transform pair relating a time-dependent function $d(t)$ to its frequency spectrum $\hat{d}(\omega)$ is defined as

$$\hat{d}(\omega) = \int_{-\infty}^{\infty} d(t) \exp(i\omega t) dt, \quad (1)$$

$$d(t) = \frac{1}{2\pi} \int_{-\infty}^{\infty} \hat{d}(\omega) \exp(-i\omega t) d\omega, \quad (2)$$

where i is the imaginary unit and ω denotes the angular frequency. The integration limits in equation (1) can be decomposed in two time intervals, $(-\infty, 0]$ and $[0, \infty)$. According to Bleistein et al. (2001), the second interval correspond the physical condition of *causality*, that is, the source is initiated at some finite time, which we can take to be $t = 0$, before the wavefield is recorded. Correspondingly, the first interval corresponds to the physical condition of *anticausality*, i.e., the wavefield described at some time in the past implodes towards a source at time zero.

Application of the temporal Fourier transform to the acoustic wave equation with variable density leads to the corresponding Helmholtz equation, which can be written as (Bleistein et al., 2001)

$$\rho(x) \nabla \cdot \left[\frac{1}{\rho(x)} \nabla \hat{p}(x, \omega) \right] + \frac{\omega^2}{c^2(x)} \hat{p}(x, \omega) = -\hat{F}(x, \omega). \quad (3)$$

Here $\rho(x)$ denotes the variable density, $\hat{p}(x, \omega)$ the pressure field, $c(x)$ is the spatially varying wave velocity and $\hat{F}(x, \omega)$ is a source term. In the particular case of a temporal and spatial point source at position x^s , the source term is given by a delta function $\delta(x - x^s)$. Then, the pressure field is represented by the Green's function $\hat{G}(x, \omega; x^s)$, which must satisfy

$$\rho(x) \nabla \cdot \left[\frac{1}{\rho(x)} \nabla \hat{G}(x, \omega; x^s) \right] + \frac{\omega^2}{c^2(x)} \hat{G}(x, \omega; x^s) = -\delta(x - x^s). \quad (4)$$

The basis for seismic interferometry is Gauss's theorem, which relates an integral over a closed surface S of an arbitrary vector field to an integral over the enclosed volume V of the divergence of the vector field. Choosing the vector field appropriately, this theorem can be written as (Green, 1828)

$$\begin{aligned} \oint_S \frac{1}{\rho(x)} (\hat{p} \nabla \hat{G} - \hat{G} \nabla \hat{p}) \cdot \hat{n} dS &= \iiint_V \nabla \cdot \left(\frac{1}{\rho(x)} \hat{p} \nabla \hat{G} - \frac{1}{\rho(x)} \hat{G} \nabla \hat{p} \right) dV \\ &= \iiint_V \left[\hat{p} \nabla \cdot \left(\frac{1}{\rho(x)} \nabla \hat{G} \right) - \hat{G} \nabla \cdot \left(\frac{1}{\rho(x)} \nabla \hat{p} \right) \right] dV, \end{aligned} \quad (5)$$

where \hat{n} is the unit vector normal to surface S pointing into the outward direction of volume V .

Reciprocity theorems of convolution and correlation type

Following Wapenaar et al. (2010a,b), we consider two states A and B in the Helmholtz equation in order to calculate the reciprocity theorem of the convolution type. We assume both states to have the same

properties, i.e., $\rho^A(x) = \rho^B(x) = \rho(x)$ and $c^A(x) = c^B(x) = c(x)$. Moreover, we assume that the wavefields in both states have causal sources inside volume V . Since the states differ only in the source, the corresponding wavefields \hat{p}^A and \hat{p}^B must satisfy

$$\rho(x)\nabla \cdot \left[\frac{1}{\rho(x)} \nabla \hat{p}^A \right] + \frac{\omega^2}{c^2(x)} \hat{p}^A = -\hat{F}^A, \quad (6)$$

$$\rho(x)\nabla \cdot \left[\frac{1}{\rho(x)} \nabla \hat{p}^B \right] + \frac{\omega^2}{c^2(x)} \hat{p}^B = -\hat{F}^B, \quad (7)$$

Note that equations (6) and (7) show us that the difference between the state A and B is in the source distribution and the wavefield, the rest of the other properties remain the same. After multiplication of equation (6) by \hat{p}^B and (7) by \hat{p}^A , their difference yields

$$\rho(x)\hat{p}^B \nabla \cdot \left[\frac{1}{\rho(x)} \nabla \hat{p}^A \right] - \rho(x)\hat{p}^A \nabla \cdot \left[\frac{1}{\rho(x)} \nabla \hat{p}^B \right] = -\hat{p}^B \hat{F}^A + \hat{p}^A \hat{F}^B. \quad (8)$$

Adding and subtracting a term $\nabla \hat{p}^A \nabla \hat{p}^B$ on the left-hand side of equation (8), as well as manipulating and reorganizing the terms and dividing the result by $\rho(x)$, we obtain

$$\nabla \cdot \left[\frac{1}{\rho(x)} (\hat{p}^B \nabla \hat{p}^A - \hat{p}^A \nabla \hat{p}^B) \right] = \frac{1}{\rho(x)} (\hat{p}^A \hat{F}^B - \hat{p}^B \hat{F}^A). \quad (9)$$

After integration over an arbitrary volume V , equation (9) has an appropriate form to apply Gauss's theorem. The result is the reciprocity theorem of convolution type, which we can represent as

$$\oint_S \frac{1}{\rho(x)} (\hat{p}^B \nabla \hat{p}^A - \hat{p}^A \nabla \hat{p}^B) \cdot \hat{n} dS = \iiint_V \frac{1}{\rho(x)} (\hat{p}^A \hat{F}^B - \hat{p}^B \hat{F}^A) dV. \quad (10)$$

A completely analogous analysis can be carried out starting at the complex conjugate of equation (6) together with equation (7). Replacing the wavefield \hat{p}^A and the source term \hat{F}^A in the above derivation by their complex conjugates \hat{p}^{A*} and \hat{F}^{A*} , where the superscript $*$ denotes the complex conjugate, results in

$$\oint_S \frac{1}{\rho(x)} (\hat{p}^B \nabla \hat{p}^{A*} - \hat{p}^{A*} \nabla \hat{p}^B) \cdot \hat{n} dS = \iiint_V \frac{1}{\rho(x)} (\hat{p}^{A*} \hat{F}^B - \hat{p}^B \hat{F}^{A*}) dV. \quad (11)$$

This is the reciprocity theorem of correlation type.

Using the Sommerfeld radiation condition (Bleistein et al., 2001) and Wapenaar anti-radiation condition (Wapenaar, 2006), it is possible demonstrate that the left-hand side integrals in equations (10) and (11) tends to zero when the radius of the closed surface tends to infinity, respectively.

Surface decomposition of reciprocity theorems of convolution and correlation type

In this section we analyse the closed surface integrals in the reciprocity theorems of convolution and correlation type, equations (10) and (11). Since volume V is arbitrary in these equations, it can be chosen as a cylinder. Then, the surface S in equation (10) and (11) can be decomposed into three surfaces defined as $S_1 = \{(x_1, x_2, x_3) \in \mathbb{R}^2 | x_3 = x_3^1\}$, $S_2 = \{(x_1, x_2, x_3) \in \mathbb{R}^2 | x_3 = x_3^2\}$ and $S_3 = \{(x_1, x_2, x_3) \in \mathbb{R}^2 | x_3 = x_3^3\}$, with the versors $\hat{n}_1 = (0, 0, -1)$, $\hat{n}_2 = (0, 0, 1)$ and $\hat{n}_3 = (x_1, x_2, 0)$, respectively (Figure 1).

Upon this choice, the closed-surface integral in equation (10) can be recast into the form

$$\begin{aligned} & \iint_{S_1} \frac{1}{\rho(x)} (\hat{p}^B \nabla \hat{p}^A - \hat{p}^A \nabla \hat{p}^B) \cdot \hat{n}_1 dx_1 dx_2 + \iint_{S_2} \frac{1}{\rho(x)} (\hat{p}^B \nabla \hat{p}^A - \hat{p}^A \nabla \hat{p}^B) \cdot \hat{n}_2 dx_1 dx_2 + \\ & \iint_{S_3} \frac{1}{\rho(x)} (\hat{p}^B \nabla \hat{p}^A - \hat{p}^A \nabla \hat{p}^B) \cdot \hat{n}_3 dx_1 dx_2 = 0. \end{aligned} \quad (12)$$

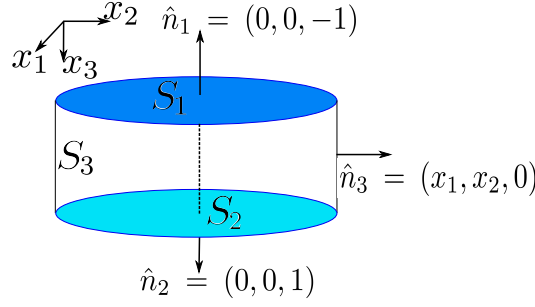


Figure 1: Cylinder surface decomposed into three surfaces, S_1 , S_2 and S_3 .

The Sommerfeld radiation conditions require that the integral over surface S_3 tends to zero when the cylindrical radius tends to infinity. Thus, we conclude that the integrals over surfaces S_1 and S_2 must satisfy

$$\iint_{S_1} \frac{1}{\rho(x)} (\hat{p}^B \nabla \hat{p}^A - \hat{p}^A \nabla \hat{p}^B) \cdot \hat{n}_1 dx_1 dx_2 = - \iint_{S_2} \frac{1}{\rho(x)} (\hat{p}^B \nabla \hat{p}^A - \hat{p}^A \nabla \hat{p}^B) \cdot \hat{n}_2 dx_1 dx_2, \quad (13)$$

where S_1 and S_2 now denote the complete horizontal planes at $x_3 = x_3^1$ and $x_3 = x_3^2$, respectively. To derive equation (13), no assumptions regarding the nature of the medium inside and outside the surface S were necessary. In other words, this equation is valid for general inhomogeneous media, as long as the sources are outside volume V and the medium properties in both states are the same inside the volume.

For the reciprocity theorem of correlation type, the analogous procedure provides

$$\begin{aligned} & \iint_{S_1} \frac{1}{\rho(x)} (\hat{p}^B \nabla \hat{p}^{A*} - \hat{p}^{A*} \nabla \hat{p}^B) \cdot \hat{n}_1 dx_1 dx_2 + \iint_{S_2} \frac{1}{\rho(x)} (\hat{p}^B \nabla \hat{p}^{A*} - \hat{p}^{A*} \nabla \hat{p}^B) \cdot \hat{n}_2 dx_1 dx_2 + \\ & \iint_{S_3} \frac{1}{\rho(x)} (\hat{p}^B \nabla \hat{p}^{A*} - \hat{p}^{A*} \nabla \hat{p}^B) \cdot \hat{n}_3 dx_1 dx_2 = 0. \end{aligned} \quad (14)$$

Then form of the integral over surface S_3 in equation (14) does not allow for the application of the Sommerfeld radiation conditions. However, using the ‘‘Wapenaar anti-radiation conditions’’ (Wapenaar, 2006), we can also justify that this integral tends to zero when the cylinder radius tends to infinity. In effect, these conditions state that there should be no contributions from infinity to this integral in an inhomogeneous medium with sufficient scattering. Hence, the reciprocity theorem of correlation type can be written as

$$\iint_{S_1} \frac{1}{\rho(x)} (\hat{p}^B \nabla \hat{p}^{A*} - \hat{p}^{A*} \nabla \hat{p}^B) \cdot \hat{n}_1 dx_1 dx_2 = - \iint_{S_2} \frac{1}{\rho(x)} (\hat{p}^B \nabla \hat{p}^{A*} - \hat{p}^{A*} \nabla \hat{p}^B) \cdot \hat{n}_2 dx_1 dx_2, \quad (15)$$

again with S_1 and S_2 denoting the complete horizontal planes at $x_3 = x_3^1$ and $x_3 = x_3^2$. Equation (15) is valid for general inhomogeneous media inside and outside the surface S , as long as the medium inside the cylinder is sufficiently inhomogeneous at far distances for the scattering to satisfy the Wapenaar anti-radiation conditions.

One-way wavefield decomposition

To derive the one-way forms of the above reciprocity theorems, we consider the two states, A and B , in the situation depicted in Figure 2. The surfaces S_1 and S_2 have now been extended to cover full horizontal planes, i.e., they are now defined as $\partial D_1 = \{(x_1, x_2, x_3) \in \mathbb{R}^3 | x_3 = x_3^1\}$ and $\partial D_2 = \{(x_1, x_2, x_3) \in \mathbb{R}^3 | x_3 = x_3^2\}$. Both states A and B have source positions at surface ∂D_1 , in x^A and x^B , respectively, and the receivers are distributed over both surfaces. Note that we do not consider ∂D_1 to be a free surface.

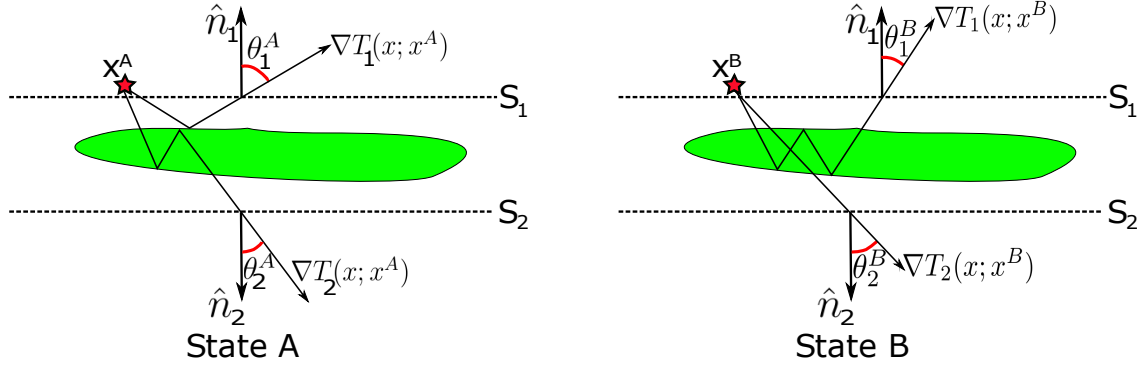


Figure 2: Sketch of two sources at positions x^A and x^B at surface ∂D_1 with receivers along the both surfaces ∂D_1 and ∂D_2 . Also shown are selected propagation paths to selected receivers and the angles between the propagation directions and the surface normals at these receivers.

According to Wapenaar and Berkhout (1989) the total wavefield $\hat{p}(x, \omega)$ at the receiver can be decomposed in up- (–) and downgoing (+) constituents, i.e.,

$$\hat{p}(x, \omega) = \hat{p}_+(x, \omega) + \hat{p}_-(x, \omega). \quad (16)$$

Equation (16) is important, because this decomposition allows to derive the one-way reciprocity theorems of convolution and correlation type. These, in turn, are the basis for the retrieval of the up- and downgoing Green's functions using least squares inversion.

At this point, we suppose that the sources are delta functions in space and time, and that the velocity field is sufficiently smooth in a small region around both surfaces ∂D_1 and ∂D_2 . Under these assumptions, we can express the up- and downgoing pressure fields $\hat{p}_\pm(x, \omega; x^s)$ as the ray-theoretical approximation of the Green's function, which form is given by the following expression

$$\hat{p}_\pm(x, \omega; x^s) = A(x; x^s) \exp[\mp i\omega T(x; x^s)], \quad (17)$$

where T is the traveltime function that satisfies the eikonal equation $\|\nabla T(x; x^s)\|^2 = \frac{1}{c^2(x)}$, the subscript \pm in equation (17) indicates the down- and upgoing wavefield direction, respectively, and $A(x; x^s)$ is the amplitude, principally determined by the geometrical-spreading factor. Signs (–) and (+) in the exponential factor in equation (17) refer to causal and anticausal responses in the time domain, respectively. In high-frequency approximation, the derivative of equation (17) can be represented as

$$\nabla \hat{p}_\pm \approx \mp i\omega \hat{p}_\pm \nabla T(x; x^s), \quad (18)$$

where the amplitude variation has been neglected.

One-way reciprocity theorems of convolution and correlation type

In this section we derive the one-way reciprocity theorems of convolution and correlation type using the above wavefield decomposition. These theorems are helpful to extract detailed information about the waves and their behaviour as a function of the propagation direction. When the wavefield is decomposed into up- and downgoing components, the gradients of these individual wavefield components depend on the propagation direction.

We start our derivation at the one-way reciprocity theorem of convolution type, equation (13). Replacing the wavefield in equation (13) by its decomposed form according to expression (16), we obtain

$$\begin{aligned} & \iint_{\partial D_1} \frac{1}{\rho(x)} [(\hat{p}_+^B + \hat{p}_-^B) \nabla (\hat{p}_+^A + \hat{p}_-^A) - (\hat{p}_+^A + \hat{p}_-^A) \nabla (\hat{p}_+^B + \hat{p}_-^B)] \cdot \hat{n}_1 dx_1 dx_2 = \\ & - \iint_{\partial D_2} \frac{1}{\rho(x)} [(\hat{p}_+^B + \hat{p}_-^B) \nabla (\hat{p}_+^A + \hat{p}_-^A) - (\hat{p}_+^A + \hat{p}_-^A) \nabla (\hat{p}_+^B + \hat{p}_-^B)] \cdot \hat{n}_2 dx_1 dx_2. \end{aligned} \quad (19)$$

Assuming that the medium is smooth in a small region around ∂D_1 and ∂D_2 , the normal derivatives of the Green's functions can be approximated in high frequency using expression (18). Still upon high-frequency arguments, the main contributions to the integrals in equation (19) come from the stationary points on surfaces ∂D_1 and ∂D_2 . At those stationary points, the absolute values of the cosines of the ray angles for \hat{p}^A and \hat{p}^B are identical. This implies, for example, that the terms $\hat{p}_+^B \nabla \hat{p}_+^A$ and $\hat{p}_+^B \nabla \hat{p}_+^A$ give equal contribution to the integral, whereas the contributions of $-\hat{p}_+^B \nabla \hat{p}_+^A$ and $\hat{p}_+^A \nabla \hat{p}_+^B$ cancel each other (Wapenaar and Fokkema, 2006). Hence, we can rewrite equation (19) as

$$\iint_{\partial D_1} \frac{1}{\rho(x)} (\hat{p}_+^B \nabla \hat{p}_+^A - \hat{p}_-^B \nabla \hat{p}_+^A) \cdot \hat{n}_1 dx_1 dx_2 \approx - \iint_{\partial D_2} \frac{1}{\rho(x)} (\hat{p}_+^B \nabla \hat{p}_-^A - \hat{p}_-^B \nabla \hat{p}_+^A) \cdot \hat{n}_2 dx_1 dx_2. \quad (20)$$

Since surfaces ∂D_1 and ∂D_2 have the geometrical disposition shown in Figure 2, the versors in equation (20) can be expressed as $\hat{n}_1 = (0, 0, -1)$ and $\hat{n}_2 = (0, 0, 1)$, allowing us to express equation (20) as

$$\iint_{\partial D_1} \frac{1}{\rho(x)} (\hat{p}_+^B \partial_3 \hat{p}_+^A - \hat{p}_-^B \partial_3 \hat{p}_+^A) dx_1 dx_2 \approx \iint_{\partial D_2} \frac{1}{\rho(x)} (\hat{p}_+^B \partial_3 \hat{p}_-^A - \hat{p}_-^B \partial_3 \hat{p}_+^A) dx_1 dx_2, \quad (21)$$

where ∂_3 denotes the derivative in the vertical direction. Equation (21) is the most common form to write the one-way reciprocity theorem of convolution type.

As before, the derivation of the one-way reciprocity theorem of correlation type follows an analogous path. For this purpose, we need the complex conjugate of expression (16) to replace the full wavefield in equation (15) by its decomposed expression. Also using the complex conjugate of equation (18), we find

$$\begin{aligned} & \iint_{\partial D_1} \frac{1}{\rho(x)} [(\hat{p}_+^B + \hat{p}_-^B) \nabla (\hat{p}_+^{A*} + \hat{p}_-^{A*}) - (\hat{p}_+^{A*} + \hat{p}_-^{A*}) \nabla (\hat{p}_+^B + \hat{p}_-^B)] \cdot \hat{n}_1 dx_1 dx_2 = \\ & - \iint_{\partial D_2} \frac{1}{\rho(x)} [(\hat{p}_+^B + \hat{p}_-^B) \nabla (\hat{p}_+^{A*} + \hat{p}_-^{A*}) - (\hat{p}_+^{A*} + \hat{p}_-^{A*}) \nabla (\hat{p}_+^B + \hat{p}_-^B)] \cdot \hat{n}_2 dx_1 dx_2. \end{aligned} \quad (22)$$

Again, the principal contributions to the integrals in equation (22) come from the stationary points on surfaces ∂D_1 and ∂D_2 . This implies, for example, that the terms $\hat{p}_+^B \nabla \hat{p}_+^{A*}$ and $\hat{p}_+^{A*} \nabla \hat{p}_+^B$ give equal contribution to the integral, whereas the contributions of $\hat{p}_+^B \nabla \hat{p}_+^{A*}$ and $-\hat{p}_-^{A*} \nabla \hat{p}_+^B$ cancel each other (Wapenaar and Fokkema, 2006). With these results, we can write equation (22) as

$$\iint_{\partial D_1} \frac{1}{\rho(x)} (\hat{p}_+^B \nabla \hat{p}_+^{A*} - \hat{p}_-^B \nabla \hat{p}_-^{A*}) \cdot \hat{n}_1 dx_1 dx_2 \approx - \iint_{\partial D_2} \frac{1}{\rho(x)} (\hat{p}_+^B \nabla \hat{p}_+^{A*} - \hat{p}_-^B \nabla \hat{p}_-^{A*}) \cdot \hat{n}_2 dx_1 dx_2. \quad (23)$$

Finally, using the explicit form of the versors values $\hat{n}_1 = (0, 0, -1)$ and $\hat{n}_2 = (0, 0, 1)$, we can express equation (23) as

$$\iint_{\partial D_1} \frac{1}{\rho(x)} (\hat{p}_+^B \partial_3 \hat{p}_+^{A*} - \hat{p}_-^B \partial_3 \hat{p}_-^{A*}) dx_1 dx_2 \approx \iint_{\partial D_2} \frac{1}{\rho(x)} (\hat{p}_+^B \partial_3 \hat{p}_+^{A*} - \hat{p}_-^B \partial_3 \hat{p}_-^{A*}) dx_1 dx_2. \quad (24)$$

Equation (24) is the most common form to write the one-way reciprocity theorem of correlation type.

Up- and downgoing Green's functions

Using the reciprocity theorems of convolution and correlation type, it is possible to retrieve the up- and downward propagating wavefields at an arbitrary datum in depth. For this purpose, we still need an additional relationship, previously derived by van der Neut et al. (2015a).

To derive this relationship in our notation, we start again at two states, A and B (indicated by superscripts A and B) in the frequency-space domain (Figure 3).

In state A , we consider a point source positioned immediately above surface ∂D_1 . In this situation, the vertical derivative of the downgoing wavefield at the surface can be expressed as $\partial_3 \hat{p}_+^A = \delta(x - x^A)$

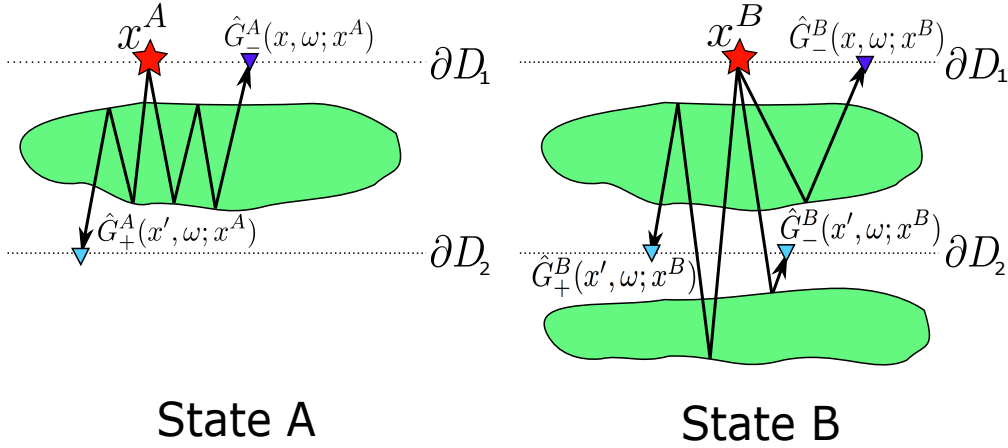


Figure 3: Two wavefield states in an inhomogeneous overburden. State A is used to describe the transmitted wavefield from the surface and its responses recorded at the datum and at the surface. State B is used to describe the total wavefield taking into account all events propagating in the medium.

(Wapenaar et al., 2014a). The validity region of this expression in state A is limited by surfaces ∂D_1 and ∂D_2 . Between these surfaces, the medium may be arbitrarily inhomogeneous. Above ∂D_1 and below ∂D_2 we consider homogeneous halfspaces without a free surface (Figure 3).

In state B, we consider the same inhomogeneous medium between surfaces ∂D_1 and ∂D_2 as in state A. Above ∂D_1 , we still consider a homogeneous medium halfspace without a free surface, and below ∂D_2 we now consider a scattering body. The source in state B is also a point source immediately above surface ∂D_1 , such that the vertical derivative of the downgoing wavefield can be represented as $\partial_3 \hat{p}_+^B = \delta(x - x^B)$ (Wapenaar et al., 2014a).

In both states A and B, we consider the wavefield decomposition into up- and downgoing constituents in analogy to equation (16). An analysis of the physical situation in both states allows for an interpretation of all propagating events at every surface in Figure 3, resulting in Table 1.

Table 1: Analysis of the up- and downgoing wavefields at surfaces ∂D_1 and ∂D_2 in states A and B, respectively.

Surface	Direction	Wavefield in State A	Wavefield in State B
∂D_1	+	point source in x^A	point source in x^B
∂D_1	-	$\hat{G}_-^A(x, \omega; x^A)$	$\hat{G}_-^B(x, \omega; x^B)$
∂D_2	+	$\hat{G}_+^A(x', \omega; x^A)$	$\hat{G}_+^B(x', \omega; x^B)$
∂D_2	-	0	$\hat{G}_-^B(x', \omega; x^B)$

Substitution of the wavefield expressions from Table 1 in the one-way reciprocity theorem of convolution type (equation 21) leads to

$$\frac{1}{\rho(x^A)} \hat{G}_-^B(x^A, \omega; x^B) - \frac{1}{\rho(x^B)} \hat{G}_-^A(x^B, \omega; x^A) \approx \iint_{\partial D_2} \frac{1}{\rho(x)} \hat{G}_-^B(x', \omega; x^B) \partial_3 \hat{G}_+^A(x', \omega; x^A) d^2 x', \quad (25)$$

where we have carried out the integrations over the delta functions describing the vertical derivatives of the point-source wavefields on the right-hand side.

Equation (25) is the first of our main results. This expression allows us to invert for the upgoing Green's function $\hat{G}_-^B(x', \omega; x^B)$ at the datum ∂D_2 if we know the corresponding Green's function $\hat{G}_-^A(x^A, \omega; x^B)$ at the surface ∂D_1 , as long as we have sufficient information on the inhomogeneous medium between the two surfaces to model the terms $\frac{1}{\rho(x^B)} \hat{G}_-^A(x^B, \omega; x^A)$ and $\frac{1}{\rho(x)} \partial_3 \hat{G}_+^A(x', \omega; x^A)$.

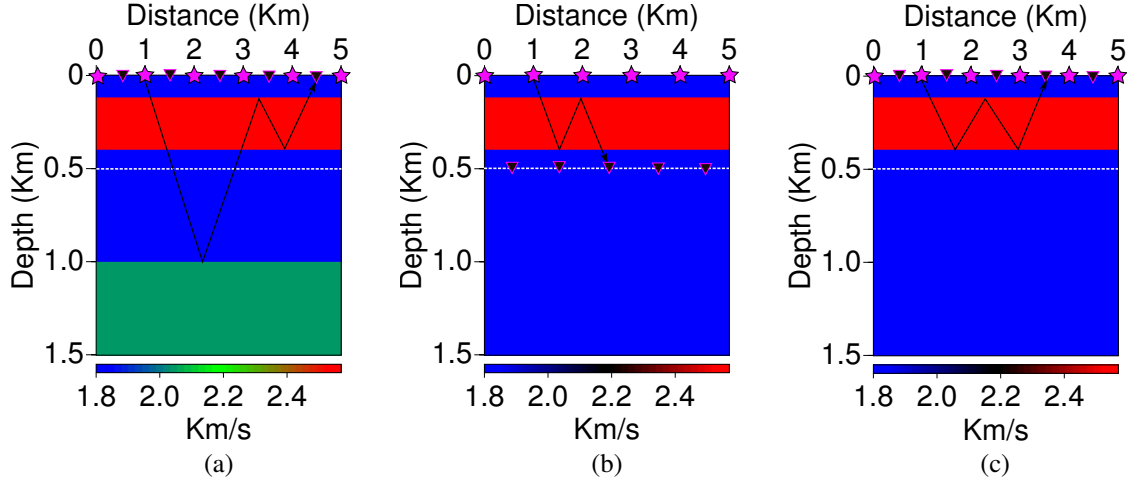


Figure 4: Model and acquisition geometry for the synthetic seismic data. (a) Array of sources and receivers at the surface, (b) array of shots at the surface and receivers at 500 m depth and (c) truncated medium with shots and receivers at the surface.

In analogy to this analysis, we can replace the wavefield expressions of Table 1 in the one-way reciprocity theorem of correlation type (equation 24), to obtain

$$\iint_{\partial D_2} \frac{1}{\rho(x)} \hat{G}_+^A(x', \omega; x^B) \partial_3 \hat{G}_+^{A*}(x', \omega; x^A) d^2 x' + \iint_{\partial D_1} \frac{1}{\rho(x)} \hat{G}_-^A(x, \omega; x^B) \partial_3 \hat{G}_-^{A*}(x, \omega; x^A) d^2 x - \iint_{\partial D_1} \frac{1}{\rho(x)} \hat{G}_-^B(x, \omega; x^B) \partial_3 \hat{G}_-^{A*}(x, \omega; x^A) d^2 x \approx \iint_{\partial D_2} \frac{1}{\rho(x)} \hat{G}_+^B(x', \omega; x^B) \partial_3 \hat{G}_+^{A*}(x', \omega; x^A) d^2 x', \quad (26)$$

This equation allows us to calculate the downgoing Green's function $\hat{G}_+^B(x', \omega; x^B)$ at the datum from the corresponding upgoing wavefield $\hat{G}_-^B(x', \omega; x^B)$. All that is needed for this purpose are the vertical derivatives of the transmitted wavefield from the surface down to the datum $\frac{1}{\rho(x)} \partial_3 \hat{G}_+^A(x', \omega; x^A)$ and of the truncated upgoing wavefield $\frac{1}{\rho(x)} \partial_3 \hat{G}_-^{A*}(x, \omega; x^A)$ at the surface.

RESULTS

In order to validate formulas (25) and (26), we carried out a simple numerical experiment using synthetic data.

Model

We retrieved the up- and downgoing wavefields at the datum using synthetic surface data from a horizontally layered medium (Figure 4a). The model has a width of 5 km and a depth of 1.5 km. It consists of a 1.8 km/s background velocity with a 300 m thick high-velocity layer (2.5 km/s) between the surface and the datum and an interface at 1 km depth. To further simplify things we considered the density in all layers constant.

The seismic array at the surface consisted of 201 sources spaced at 25 m, and the same number of receivers for each shot, also spaced at 25 m. The seismic array simulating the reference data at the datum consisted of 201 shots at surface and 201 receivers at the datum, both spaced at 25 m. Synthetic seismic data as input to retrieve the up- and downgoing Green's functions are the conventional seismic data recorded with shots and receivers located at the surface (Figure 4a). Auxiliary data simulated in the reference medium without the interface below the datum are (2) the transmitted wavefield with sources at surface and receivers at the datum in the reference medium (Figure 4b) and (3) the truncated wavefield with shots

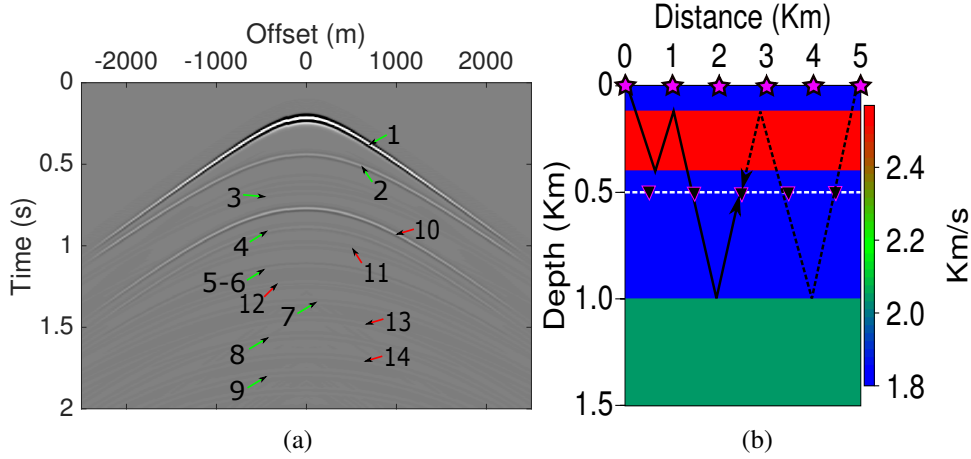


Figure 5: (a) Full synthetic seismic wavefield with its up- and downgoing constituents labelled, obtained using a (b) source array at the surface and receivers at the datum at 500 m depth in the horizontally layered model.

and receivers located at the surface (Figure 4c). The wavelet used for the numerical modelling was a Ricker wavelet of 25 Hz peak frequency.

For comparison, we also simulated the full wavefield (Figure 5a) with sources at the surface and receivers at the datum in 500 m depth (Figure 5b). The visible events in the seismic section of Figure 5a are labelled with numbers so as to identify and interpret them. To facilitate the interpretation, we used green arrows for downgoing events and red arrows for upgoing events. This will also help to compare the respective events to the inverted up- and downgoing wavefields shown below.

Event interpretation

In this section we interpret the up- and downgoing constituents of the full seismic wavefield in Figure 5a. For that purpose, we calculated the time trajectory of every event and represent it as ray path in the Figure 6. The ray paths for the visible downgoing events in Figure 5a are shown in Figure 6a, and those for the upgoing events in Figure 6b.

The zero-offset traveltimes corresponding to each event of the downgoing constituent in Figure 6a are: $t_1 = 0.23s$, $t_2 = 0.45s$, $t_3 = 0.68s$, $t_4 = 0.90s$, $t_5 = 1.12s$, $t_6 = 1.12s$, $t_7 = 1.34s$, $t_8 = 1.56s$ and $t_9 = 1.79s$. The corresponding times for the upgoing events are: $t_{10} = 0.78s$, $t_{11} = 1.01s$, $t_{12} = 1.23s$, $t_{13} = 1.45s$ and $t_{14} = 1.68s$ (Figure 6b).

Using least-squares inversion in equations (25) and (26), we can separate the total wavefield at the surface into its up- and downgoing constituents at the datum. In the numerical examples below we will associate our interpretations in Figure 6 with the up- and downgoing Green's functions retrieved by inversion.

Downgoing Green's functions

As the next step, we retrieved the downgoing constituents of the Green's function $\hat{G}_+^B(x', \omega; x^A)$ at the datum in 500 m depth by least-squares inversion applied to equation (26). For this purpose, we modelled the vertical derivative of the transmitted wavefield $\partial_3 \hat{G}_+^A(x', \omega; x^A)$ and the vertical derivative of the truncated wavefield $\partial_3 \hat{G}_-^A(x, \omega; x^A)$ in the reference model without inhomogeneity below the datum. As mentioned before, this inversion problem is ill-posed. Therefore, the least-squares inversion needs to be stabilized. We opted for a simple Tikhonov regularization and tested different values for the regularization parameter to study its influence on the inversion result.

Figure 7 shows the inverted Green's function $\hat{G}_+^B(x', \omega; x^A)$ at the datum in 500 m depth for four values of the regularization parameter. In all four sections, the kinematic properties and the relative amplitudes

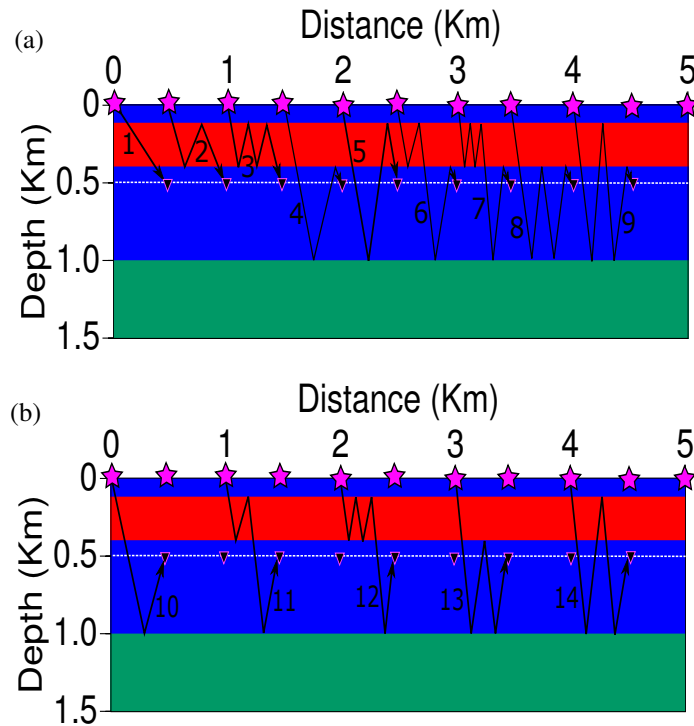


Figure 6: Model with ray paths to interpret the wavefield constituents: (a) Downgoing and (b) upgoing events.

correspond to those of the downward propagating events in Figure 5a.

For more a quantitative evaluation of the result, Figure 8 shows the central (zero-offset) traces of the four downward wavefields of Figure 7, retrieved by differently regularized inversions. Moreover, the black line in the Figure 8 is the result from synthetic modelling. Note again that the latter wavefield includes both up- and downward propagating events. For better visibility, Figure 8a shows the first 0.8 s and Figure 8b shows the part between 0.6 s and 1.4 s at a twenty times smaller scale. At this scale, numerical artefacts become visible. For the weakest regularization, their amplitude is comparable to that of the smallest events. A value of $\epsilon = 0.01\%$ is already sufficient to reduce them to an acceptable level.

We observe that the inversion results are almost indistinguishable, indicating the low influence of the regularization parameter. Comparing the modelled trace with the inverted ones, we note that events 1, 2, 4, 5 and 6 match nicely. On the other hand, event 10 is only present in the modelled result, but does not present a counterpart in the inverted traces. The reason is event 10 belongs to the upward propagating Green's functions. Therefore, its absence is the desired behaviour of the inversion. Events interpreted in Figure 6 as 3, 7, 8 and 9 do not appear in the central traces analysed here, because their amplitudes are too attenuated by the propagation effects, making them almost invisible in the zero-offset trace. Actually, these events, which correspond to second and third order multiples, could be interpreted in the sections of Figures 5 and 6 only at offsets of more than 500 m.

In summary, we see that all downward propagating events are correctly positioned in time and that the amplitudes are comparable. Moreover and most importantly, the result does not exhibit strong artefacts or non-physical events. Our inversion response nicely recovers high-quality versions of the physical events just as interpreted in Figure 6.

Upgoing Green's functions

In a corresponding way, the one-way reciprocity theorem of correlation type, equation (25), can be used to retrieve the upgoing Green's functions by means of stabilized least-squares inversion. In this case, we need to know the vertical derivative of the transmitted wavefield $\partial_3 \hat{G}_+^A(x', \omega; x^A)$ from the surface down to the

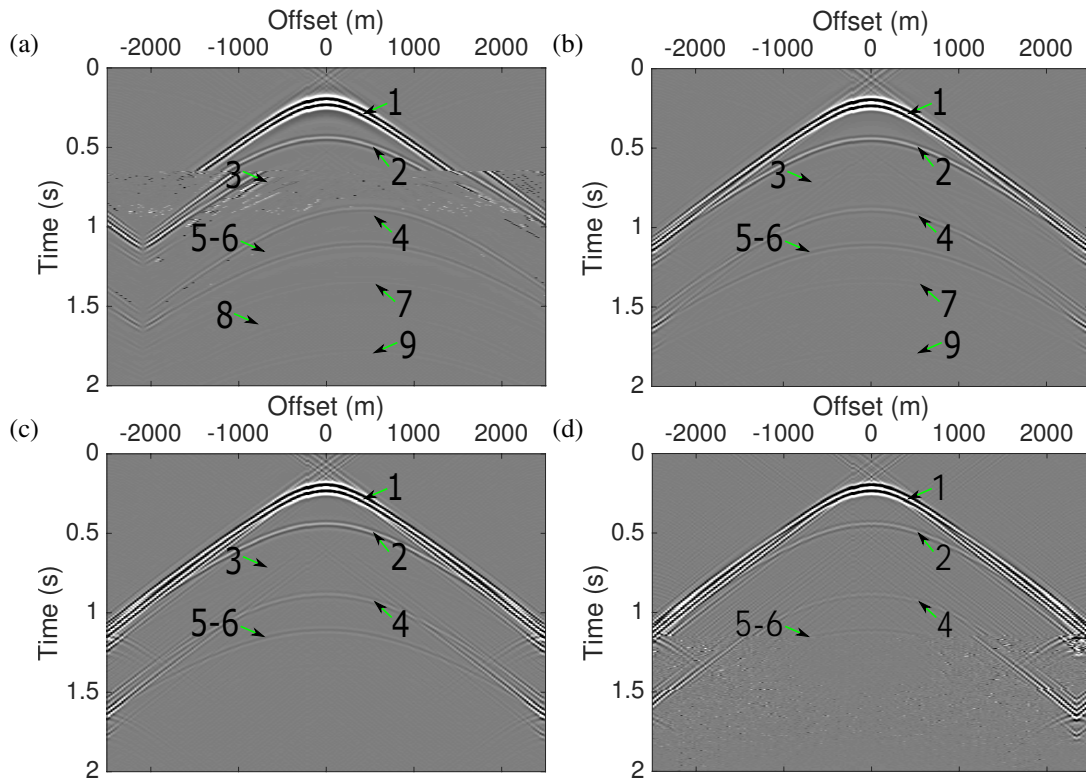


Figure 7: Downgoing Green's function $\hat{G}_+^B(x', \omega; x^A)$ at the datum in 500 m depth as retrieved by inversion, obtained using different percentages for the regularization parameter: (a) 1%, (b) 0.1%, (c) 0.01%, and (d) 0.001% of the maximum absolute value of the crosscorrelation between \hat{G}_+^A and \hat{G}_+^{A*} .

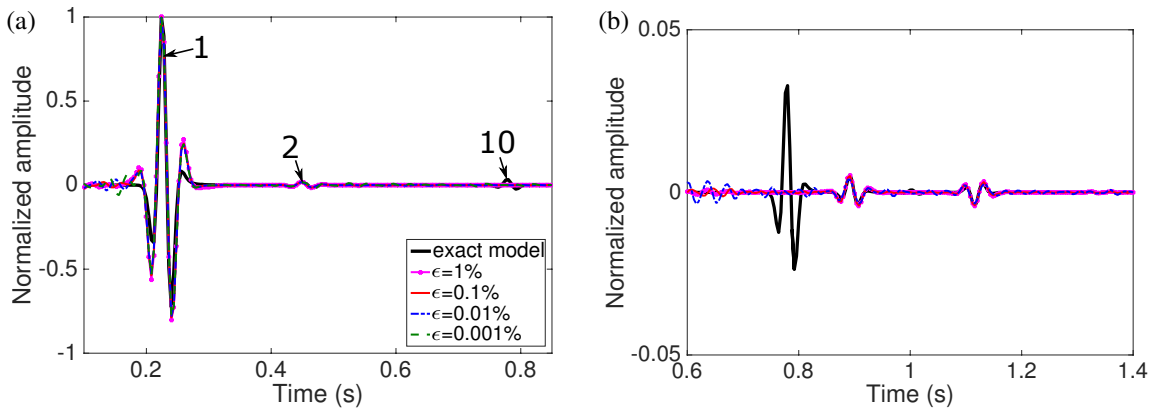


Figure 8: Central traces of the downgoing Green's functions sections in Figure 7 (coloured lines) compared to the wavefield simulated with sources at the surface and receivers at the datum (black line). (a) First part of the traces. (b) Later portion at a different scale.

datum, as well as the truncated wave field $\hat{G}_+^A(x^B, \omega; x^A)$ at the surface in the reference medium without inhomogeneity below the datum. With this information, it is possible to obtain the upward propagating Green's function $\hat{G}_-^B(x', \omega; x^B)$. Similar to the above numerical example, we tested four regularization values to retrieve different solutions of the upward Green's functions. The results are depicted in Figure 9.

We observe in Figure 9 that as desired, only the upward Green's function constituents were retrieved. A comparison to Figure 5a reveals correct positioning. Also the dynamic properties of the inverted events

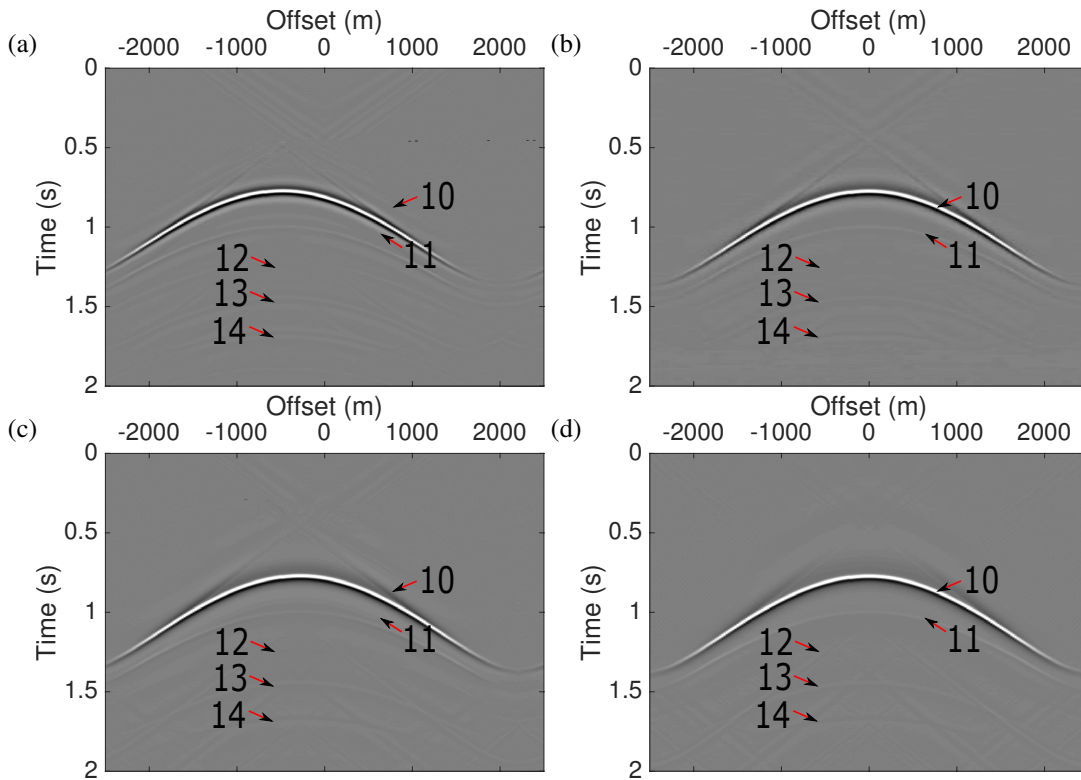


Figure 9: Upgoing Green's functions retrieved by inversion with different values for the regularization parameter: (a) 1%, (b) 0.1%, (c) 0.01%, and (d) 0.001% of the maximum absolute value of the correlation between \hat{G}_+^A and \hat{G}_+^{A*} .

largely correspond to those in the modelled section. Even event 12, which corresponds to a second order multiple and is the weakest event, is visible in the inverted sections. Moreover, except for boundary effects, no non-physical events appear in the inverted sections. This is an important advantage over correlation-based redatuming techniques (Barrera et al., 2016). As a fundamental difference with regard to the downgoing case, the effect of using different values for the regularization parameter is clearly visible. We notice differences in relative amplitudes and, most importantly, in wavelet shape.

The more quantitative analysis of the zero-offset traces (Figure 10) reveals more details. We notice the overall good match between the inverted traces and the upgoing events in the modelled data, both in traveltimes and in amplitude. On the other hand, as desired the downgoing events are absent from the inverted data. While increasing values of the regularization parameter help to better suppress the numerical artefacts, they also lead to broadened wavelets of the inverted events. Again, a value of $\epsilon = 0.01$ seems a good compromise between data quality and noise suppression.

CONCLUSIONS

In this work, we have studied a new technique to separate the wavefield into its up- and downgoing constituents. The procedure uses a more appropriate form of inverse wavefield extrapolation than correlation-based interferometric methods. It is based on the one-way reciprocity theorems of convolution and correlation type. The final expression used for the inversion has been recently derived by van der Neut et al. (2015a), who demonstrate its use for the purpose of decomposing the total wavefield at the acquisition level. Here, we rederive the underlying expression in the notation of Bleistein et al. (2001) and apply it to retrieve the Green's function constituents at a new datum level.

The wavefield decomposition proposed in this work only requires the knowledge of the transmitted wavefield from the surface down to the datum and its corresponding vertical derivative, as well as the

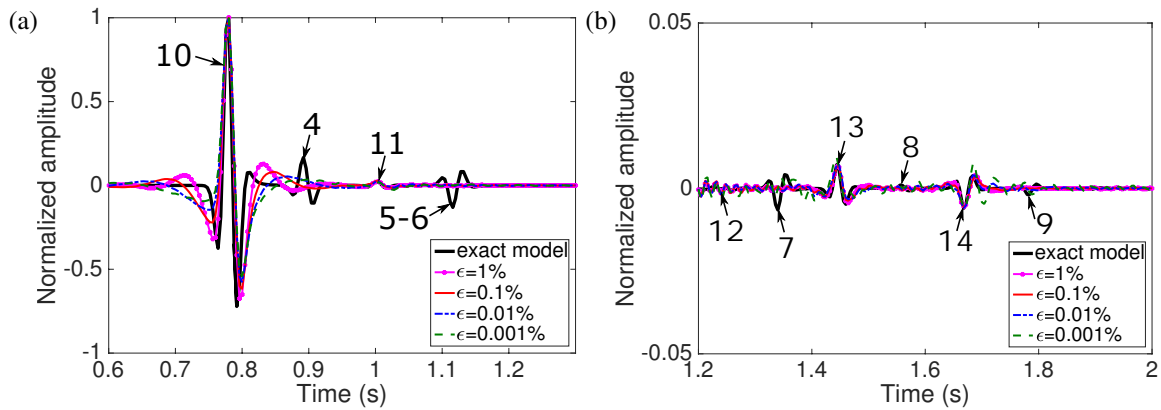


Figure 10: Central traces of the downgoing Green's functions sections in Figure 9 (coloured lines) compared to the wavefield simulated with sources at the surface and receivers at the datum (black line). (a) First part of the traces. (b) Later portion at a different scale.

truncated wavefield in a reference medium that is homogeneous below the datum and its corresponding vertical derivative. These wavefields can be determined by modelling if the medium between the surface and the datum is known with sufficient accuracy. With these input data, it is possible to retrieve the up- and downgoing constituents from the surface data.

To solve the mathematical expressions presented in this work, it is necessary to consider the solution as an inverse problem. For that purpose, we used stabilized least-squares inversion to retrieve the desired wavefield constituents. We tested the behaviour of the inversion using different values for the regularization parameter. Though the problem is ill-posed, the numerical results for the retrieved up- and downgoing wavefield constituents showed no strong dependence on the regularization parameter. All recovered wavefields matched nicely with the simulated data at the datum. In this way, we have demonstrated that all retrieved events are not only kinematically correct, but also present correct relative amplitudes. Moreover, in difference to purely correlation-based redatuming, the investigated technique has not produced non-physical events.

ACKNOWLEDGEMENTS

This work was kindly supported by the Brazilian agencies CAPES, FINEP, and CNPq, as well as Petrobras and the sponsors of the *Wave Inversion Technology (WIT) Consortium*.

REFERENCES

- Barrera, D. F., Schleicher, J., and van der Neut, J. (2016). Limitations of correlation-based redatuming methods. *WIT Report*, 20:27–41.
- Bleistein, N., Cohen, J. K., and Jr., J. W. S. (2001). *Mathematics of Multidimensional Seismic Imaging, Migration, and Inversion*. Springer.
- Green, G. (1828). *An essay on the application of mathematical analysis to the theories of electricity and magnetism*. Privately published.
- Kosloff, D. D. and Baysal, E. (1983). Migration with the full acoustic wave equation. *Geophysics*, 48:677–687.
- Schuster, G. (2009). *Seismic interferometry*. Cambridge.
- van der Neut, J., Vasconcelos, I., and Wapenaar, K. (2014). An interferometric interpretation of Marchenko redatuming. *76th EAGE Conference Exhibition*.

- van der Neut, J., Vasconcelos, I., and Wapenaar, K. (2015a). On Green's function retrieval by iterative substitution of the coupled Marchenko equations. *Geophysical Journal International*, 203:792–813.
- van der Neut, J., Wapenaar, K., Thorbecke, J., Slob, E., and Vasconcelos, I. (2015b). An illustration of adaptative marchenko imaging. *The Leading Edge*, pages 818–822.
- Wapenaar, C. P. A. and Berkhout, A. J. (1989). *Elastic Wave Field Extrapolation: Redatuming of Single- and Multi-Component Seismic Data*. Elsevier.
- Wapenaar, K. (2006). Green's function retrieval by cross-correlation in case of one-sided illumination. *Geophysical Research Letters*, 33:L19304.
- Wapenaar, K., Draganov, D., Snieder, R., Campman, X., and Verdel, A. (2010a). Tutorial on seismic interferometry: Part 1 - basic principles and applications. *Geophysics*, 75:75A195–75A209.
- Wapenaar, K. and Fokkema, J. (2006). Green's function representations for seismic interferometry. *Geophysics*, 71:SI33–SI46.
- Wapenaar, K., Slob, E., Snieder, R., and Curtis, A. (2010b). Tutorial on seismic interferometry: Part 2 - Underlying theory and new advances. *Geophysics*, 75:75A211–75A227.
- Wapenaar, K., Thorbecke, J., van der Neut, J., Broggini, F., Slob, E., and Snieder, R. (2014a). Green's function retrieval from reflection data, in absence of receiver at the virtual source position. *The Journal of the Acoustical Society of America*, 135:2847–2861.
- Wapenaar, K., Thorbecke, J., van der Neut, J., Broggini, F., Slob, E., and Snieder, R. (2014b). Marchenko imaging. *Geophysics*, 79:WA39–WA57.